Theoretical Limits of Differential Doppler Positioning Using LEO Satellite Signals

Qamar Bader*, Sharief Saleh†, Gonzalo Seco-Granados‡, and Aboelmagd Noureldin*§
*Queen's University, Kingston, ON, Canada, ‡Chalmers University of Technology, Gothenburg, Sweden,
‡Universitat Autonoma de Barcelona, Barcelona, Spain, §Royal Military College of Canada, Kingston, ON, Canada
Email: qamar.bader@queensu.ca, sharief@chalmers.se, gonzalo.seco@uab.cat, aboelmagd.noureldin@rmc.ca

GLOBECOM 2025 - 2025 IEEE Global Communications Conference | 979-8-3315-7781-0/25/$31.00 ©2025 IEEE | DOI: 10.1109/GLOBECOM59602.2025.11431750

***Abstract*—As the need for more accurate and reliable positioning systems grows, satellite-based navigation techniques are gaining significant attention, particularly those utilizing Doppler shifts from Low Earth Orbit (LEO) satellites. Traditional Doppler positioning systems often suffer from errors induced by atmospheric disturbances, satellite clock biases, and other signal impairments, especially in dynamic environments. This has motivated the exploration of differential Doppler positioning as a promising solution to mitigate these common-mode errors. This paper explores the theoretical limits of differential Doppler positioning, focusing on Doppler-only methods where position and velocity estimates are derived from Doppler measurements without relying on time-of-arrival (TOA) measurements. By leveraging the Cramér-Rao lower bound (CRLB), we provide a theoretical performance benchmark for the accuracy of position, velocity, and frequency bias estimation. Furthermore, we present a correlation model for atmospheric effects to demonstrate the impact of baseline distance on the estimation performance of differential Doppler positioning. The results show that differential Doppler positioning notably outperforms traditional non-differential Doppler positioning, particularly in low-SNR environments, with substantial gains in frequency bias, 3D velocity, and 3D position estimation accuracy.**

***Index Terms*—Atmospheric effects, Cramér-Rao lower bound (CRLB), Differential Doppler, Doppler-only positioning, LEO satellite.**

I. Introduction

The increasing demand for high-precision positioning systems has driven significant advancements in satellite-based localization techniques. In particular, Doppler-based positioning has gained attention due to its robustness in dynamic environments, such as those encountered in low Earth orbit (LEO) satellite systems [1]. Doppler shifts, caused by the relative motion between the satellite and the receiver, provide crucial information for estimating the position, velocity, and timing parameters of a user terminal (UT).

Traditional Doppler-based positioning systems, often referred to as classical methods, rely solely on measurements from the UT to estimate its state. However, these systems are susceptible to errors induced by atmospheric disturbances, carrier frequency offset (CFO), and other signal impairments [2]. To address these challenges, differential Doppler positioning has emerged as a promising approach. By leveraging additional measurements from a stationary base station (BS), which receives the same satellite signals, differential positioning can reduce the impact of common-mode errors, such as frequency biases introduced by the atmosphere or satellite clock drift.

Prior studies have leveraged LEO satellite signals for opportunistic navigation, proposing differential Doppler techniques to cancel out common errors. Authors in [3] introduce a differential Doppler framework using LEO Iridium signals with a base-rover setup, which eliminates transmitter clock bias and reduces orbit ephemeris error by differencing measurements. They analyze how baseline distance affects residual Doppler errors and derive models relating baseline length to error variance. Field experiments in this framework showed that differential Doppler positioning can reduce 3D error by nearly half compared to single-receiver methods. Likewise, the work in [4] develops a differential-LEO-augmented GNSS scheme to mitigate LEO satellite clock drift and atmospheric delay errors via single- and double-differencing between a reference and user receiver. They derive the impact of LEO orbit uncertainties on Doppler measurements and adopt an error modeling approach to remove unknown satellite clock and tropospheric delays. They further derive the Cramér–Rao lower bound (CRLB) for positioning with a hybrid LEO/GNSS constellation, providing a theoretical accuracy benchmark. However, they derive those performance bounds based on GNSS pseudorange and LEO Doppler measurements rather than Doppler-only standalone LEO positioning. They also do not explicitly model the Doppler biases or consider their correlation across the network. Other studies, [5]–[7], reported that a LEO differential navigation framework can dramatically reduce ephemeris, clock, and propagation errors. They highlight the significant performance gains obtainable by error-mitigating differencing in LEO-based positioning. However, their work did not delve into the fundamental performance limits of the system.

This work was supported by grants from the Natural Sciences and Engineering Research Council of Canada (NSERC) under grant numbers: ALLRP-560898-20 and RGPIN-2020-03900, and in part by the Spanish R+D project PID2023-152820OB-I00 and the Catalan AGAUR-ICREA Academia Program.

In this work, we analyze the theoretical limits of differential Doppler positioning using LEO satellite signals. We focus specifically on Doppler-only positioning, where the position and velocity estimates are derived solely from Doppler measurements, without the need for time-of-arrival (TOA) measurements. We explore the performance of both classical and differential Doppler positioning methods, considering various factors such as signal-to-noise ratio (SNR), baseline distance between the BS and UT, and atmospheric error models. In contrast to the work done in [3], which began directly from a differential Doppler measurement model, this work derives the CRLB from a parametric received signal model. This allows us to capture the influence of key channel parameters and their coupling with user state variables, enabling a more accurate and comprehensive performance analysis of Doppler-based positioning systems.

II. System Model and Problem Formulation

A. System Model

We consider a three-dimensional (3D) scenario consisting of a single mobile UT with unknown position $\boldsymbol{r}_u = [x_u, y_u, z_u]^\top$ and velocity $\boldsymbol{v}_u = [v_{x_u}, v_{y_u}, v_{z_u}]^\top$; a single base station (BS) with known position $\boldsymbol{r}_b = [x_b, y_b, z_b]^\top$; and I LEO satellites with known location $\boldsymbol{r}_{s,i} = [x_s^i, y_s^i, z_s^i]^\top$ and velocity $\boldsymbol{v}_s, i = [v_{x_s}^i, v_{y_s}^i, v_{z_s}^i]^\top$, where i denotes the satellite index. The receivers—both the UT and the BS—have established communication links with the I satellites.

The UT and the BS are each equipped with a single omnidirectional antenna, whereas each LEO satellite is equipped with a single directional antenna. Each LEO satellite transmits L downlink orthogonal frequency-division multiplexing (OFDM) symbols using a dedicated subset of the K total subcarriers, with a subcarrier spacing Δf. That is, the I satellites are *frequency-multiplexed*, each occupying a distinct, non-overlapping group of subcarriers (e.g., FDMA). The OFDM symbol duration is given by $T_{\text{sym}} = T + T_{\text{CP}}$, where $T = 1/\Delta f$ is the useful symbol duration, and T_{CP} is the cyclic prefix duration. The discrete-time received signal at the n^{th} receiver (where $n \in \{u, b\}$) is modeled as the superposition of signals from I LEO satellites [8]

$$y_n^{k,l} = \sum_{i=1}^{I} H_{n,i}^{k,l}\, x_i^{k,l} + \omega_n^{k,l}, \tag{1}$$

where $k = 0, \ldots, K-1$ and $l = 0, \ldots, L-1$ index the subcarrier and OFDM symbol, respectively; and $x_i^{k,l} \in \mathbb{C}$ is the transmitted pilot symbol, which is zero outside the subcarrier set assigned to satellite i. The channel model $H_n^{k,l}$ between the i^{th} LEO satellite, and the nth receiver is defined as

$$H_{n,i}^{k,l} = \alpha_{n,i} e^{-j2\pi k \Delta f (\tau_{n,i} - \nu_{n,i} l T_{\text{sym}})} e^{j2\pi f_c \nu_{n,i} l T_{\text{sym}}}, \tag{2}$$

where $\alpha_{n,i} \in \mathbb{C}$ is the complex channel gain, $\tau_{n,i}$ is the time delay, $\nu_{n,i}$ is the Doppler shift factor, and $\omega_n^{k,l} \in \mathbb{C}$ is the complex additive white Gaussian noise (AWGN) at the receiver, modeled as $\omega_n^{k,l} \sim \mathcal{CN}(0, \sigma_n^2)$, where σ_n^2 denotes the noise variance. In (2), we assume that the fast-time Doppler effect is negligible, i.e. $f_c\, \nu_{n,i}\, T \ll 1$. Here,

$$\tau_{n,i} = \frac{d_{n,i}}{c} + \delta t_{n,i}, \tag{3}$$

is the propagation delay as evaluated at the beginning of the L-symbol observation period, $d_{n,i}$ is the 3D distance between the i^{th} satellite and the n^{th} receiver, and $\delta t_{n,i}$ aggregates delays caused by clock bias and atmospheric effects. The Doppler shift factor for each link is expressed as

$$\nu_{n,i} = -\frac{(\boldsymbol{v}_{s,i} - \boldsymbol{v}_n)^\top \boldsymbol{u}_{n,i}}{c} + \delta f_{n,i}^a + \delta f_{n,i}^c, \tag{4}$$

where,

$$\boldsymbol{u}_{n,i} = \frac{\boldsymbol{r}_{s,i} - \boldsymbol{r}_n}{\|\boldsymbol{r}_{s,i} - \boldsymbol{r}_n\|}, \tag{5}$$

is the line-of-sight unit vector pointing from the n^{th} receiver towards the i^{th} satellite; $\delta f_{n,i}^c$ represents carrier frequency offset (CFO) of the $i-n$ link; and $\delta f_{n,i}^a$ aggregates the *correlated* atmospheric frequency biases between the two receivers

$$\delta f_{n,i}^a = f_{n,i}^I + f_{n,i}^T \tag{6}$$

where $f_{n,i}^I$ is the ionosphere-induced frequency error, and $f_{n,i}^T$ is troposphere-induced frequency error[1].

B. Differential Doppler Positioning Principle

We form a differential Doppler measurement by subtracting the Doppler observed at the BS from that observed at the UT

$$\Delta\nu_i = \nu_{u,i} - \nu_{b,i}. \tag{7}$$

Expanding the Doppler shift factor terms yields

$$\Delta\nu_i = \underbrace{f_{u,i}^g - f_{b,i}^g}_{\text{geometry}} + \underbrace{\delta f_{u,i}^I - \delta f_{b,i}^I}_{\approx 0} + \underbrace{\delta f_{u,i}^T - \delta f_{b,i}^T}_{\approx 0} + \underbrace{\delta f_{u,i}^c - \delta f_{b,i}^c}_{\text{UT CFO}},$$

where $f_{n,i}^g$ is the theoretical Doppler shift due to the relative radial velocities of the $i-n$ link. Ionospheric and tropospheric propagation effects are known to introduce slowly varying and spatially correlated Doppler shifts that can bias Doppler-based position estimates [9]. These effects vary with elevation angle, local weather and humidity, and diurnal/seasonal cycles, but tend to be similar for receivers that are relatively close in distance (e.g., within tens of kilometers [10], [11]). Therefore, when the two receivers are located in the vicinity of each other, these atmospheric effects can be significantly reduced through differencing.

[1]We assume that the satellites and the BS are synchronized in frequency among each other (e.g. $\delta f_{b,i}^c = 0$).

C. Atmospheric-Induced Frequency Error Modeling

We compute the instantaneous frequency error induced by the ionosphere and troposphere. All quantities are computed for a static snapshot in time, assuming no horizontal motion of the atmospheric layers (i.e., neglecting advection effects). We also assume a thin-shell approximation for the ionosphere and an exponential scale-height model for the troposphere.

The ionosphere frequency shift, $f^I_{n,i}$, is characterized by the total electron content (TEC) rate. Let $\dot{\mathrm{TEC}}_{n,i}$ denote the time derivative of the total $\mathrm{TEC}_{n,i}$ at the receiver location

$$\dot{\mathrm{TEC}}_{n,i} \;=\; \frac{d\,\mathrm{TEC}_{n,i}}{dt}\Big|_{\mathrm{n}}. \tag{8}$$

Converting to electrons m^{-2} s^{-1} via $1\,\mathrm{TECU} = 10^{16}\,\mathrm{el/m}^2$, the ionospheric frequency shift according to the Klobucher model [12] at each receiver can be modeled as

$$f^I_{n,i} = \frac{40.3}{c\,f_c}\left(\dot{\mathrm{TEC}}_{n,i}\times 10^{16}\right) m_{n,i}, \tag{9}$$

where, $m_{n,i} = \frac{1}{\sin e_{n,i}}$ is the slant-mapping factor of the receiver, and $e_{n,i}$ is the corresponding elevation angle between the satellite and the receiver.

Tropospheric frequency errors, $f^T_{n,i}$, on the other hand, are modeled following the Saastamoinen model [13]

$$f^T_{n,i} = -\frac{f_c}{c}\, m_{n,i}\, \dot{Z}_{n,i}. \tag{10}$$

where $\dot{Z}_{n,i}$ is the zenith wet-delay rate at the receiver position. We adopt an exponential model for the zenith wet-delay rate $\dot{Z}_{n,i}$ as a function of receiver height h_n

$$\dot{Z}_{n,i} = \dot{Z}_w(0)\, e^{\frac{-h_n}{H}}, \tag{11}$$

where $\dot{Z}_w(0)$ is the wet-delay rate at sea level and H the water-vapour scale height.

III. Differential Doppler Fundamental Bounds Analysis

A. Cramér-Rao Lower Bounds Analysis

To understand the fundamental performance limits of the proposed differential Doppler positioning system, we employ CRLB analysis. The CRLB provides a lower bound on the variance of any unbiased estimator, offering a theoretical benchmark for evaluating the accuracy of position, velocity, and frequency bias under a given signal and system conditions. In this context, the CRLB is derived based on a parametric signal model (2) that captures the relationship between the received signal and key channel parameters, such as Doppler shift, signal delay, and complex channel gain, as observed at both the UT and the BS.

Notation remark: The subsequent derivations apply equally to both the satellite–user (su) and satellite–base station (sb) links associated with the i^{th} satellite. To improve readability and reduce notational clutter, we omit the user/base subscripts (e.g., *u*, *b*) and the satellite index superscript (e.g., i) when the context is unambiguous. All quantities should be interpreted generically unless explicitly stated otherwise.

First, we define a vector $\boldsymbol{\eta}_{\text{ch}}$ comprising the unknown channel parameters $\boldsymbol{\eta}_{\text{ch}} = [\Re(\alpha),\ \Im(\alpha),\ \tau,\ \nu]^\top$. The Fisher information matrix (FIM) of the channel parameters can be computed as

$$\boldsymbol{J}_{\text{ch}} = \frac{2}{\sigma^2}\sum_{l=0}^{L-1}\sum_{k=0}^{K-1}\Re\left\{\left(\frac{\partial\zeta^{k,l}}{\partial\boldsymbol{\eta}_{\text{ch}}}\right)^H\left(\frac{\partial\zeta^{k,l}}{\partial\boldsymbol{\eta}_{\text{ch}}}\right)\right\}, \tag{12}$$

where $\zeta = \alpha^{k,l}\,\gamma^{k,l}$ is the noise-free term of the received signal model in (1), $(.)^H$ is the Hermitian operator, $\boldsymbol{J}_{\boldsymbol{\eta}_{\text{ch}}} \in \mathbb{R}^{4\times4}$. The partial derivatives of $\zeta^{k,l}$ with respect to $\boldsymbol{\eta}_{\text{ch}}$ are computed as $\frac{\partial\zeta^{k,l}}{\partial\Re(\alpha)} = \gamma^{k,l}$, $\frac{\partial\zeta^{k,l}}{\partial\Im(\alpha)} = j\gamma^{k,l}$, $\frac{\partial\zeta^{k,l}}{\partial\tau} = -j2\pi\alpha k\Delta f\gamma^{k,l}$, $\frac{\partial\zeta^{k,l}}{\partial\nu} = j2\pi l T_{\text{sym}}\alpha(k\Delta f + f_c)\gamma^{k,l}$, where, $\gamma^{k,l} = e^{-j2\pi k\Delta f(\tau-\nu l T_{\text{sym}})}e^{j2\pi\nu f_c l T_{\text{sym}}}x^{k,l}$. Subsequently, the corresponding state FIM $\boldsymbol{J}_{\text{state}}$ is derived as follows

$$\boldsymbol{J}_{\text{state}} = \boldsymbol{T}^\top\boldsymbol{J}_{\text{ch}}\boldsymbol{T}, \tag{13}$$

where $\boldsymbol{T}\in\mathbb{C}^{4\times N}$ (with N the dimension of the state vector, i.e. $N=11$ for the UT and $N=4$ for the BS) is defined as

$$\boldsymbol{T} = \frac{\partial\boldsymbol{\eta}_{\text{ch}}}{\partial\boldsymbol{\eta}_{\text{state}}}, \tag{14}$$

where, $\boldsymbol{\eta}^u_{\text{state}} = [\Re(\alpha),\ \Im(\alpha),\ \tau_u,\ \boldsymbol{r}_u,\ \boldsymbol{v}_u,\ \delta f^c_u,\ \delta f^a_u]^\top \in \mathbb{R}^{11}$, and, $\boldsymbol{\eta}^b_{\text{state}} = [\Re(\alpha),\ \Im(\alpha),\ \tau_b,\ \delta f^a_b]^\top \in \mathbb{R}^4$. It is important to note that although the path delay τ_u has a true geometric dependency on the user position (in a full TOA/Doppler model), we instead do not utilize the positional information of the delay, i.e., $\frac{\partial\tau_u}{\partial\boldsymbol{r}_u} = \mathbf{0}$. This ensures that the resulting position-domain FIM reflects *only* Doppler-based information. Physically, this corresponds to a Doppler-only positioning assumption, wherein no timing (TOA) information is exploited and all geometric sensitivity arises solely from carrier-frequency shifts.

To enable a solution to the formulated positioning problem, both receivers must maintain simultaneous connectivity to at least seven common LEO satellites. Accordingly, the CRLB derivation is extended to account for observations from multiple LEO satellites. Assuming independent downlink signals are received from I satellites, the FIM in the channel parameter domain is constructed as a block-diagonal composition of the individual satellite FIMs $\boldsymbol{J}^{\text{total}}_{\text{ch}} = \text{blkdiag}(\boldsymbol{J}^{(1)}_{\text{ch}}, \boldsymbol{J}^{(2)}_{\text{ch}}, \ldots, \boldsymbol{J}^{(I)}_{\text{ch}})$, where $\boldsymbol{J}^{(i)}_{\text{ch}} \in \mathbb{R}^{4\times4}$ denotes the FIM associated with the i^{th} satellite, computed using the formulation described in (12).

Let $\tilde{\boldsymbol{\eta}}_{\text{ch}} = [\boldsymbol{\eta}^\top_{\text{ch},1}, \ldots, \boldsymbol{\eta}^\top_{\text{ch},I}]^\top$ with $\boldsymbol{\eta}_{\text{ch},i} = [\Re(\alpha_i),\ \Im(\alpha_i),\ \tau_i,\ \nu_i]^\top$. $\tilde{\boldsymbol{\eta}}^u_{\text{state}} = [\boldsymbol{\gamma}^\top, \boldsymbol{\theta}_p^\top]^\top$, and $\tilde{\boldsymbol{\eta}}^b_{\text{state}} = [\boldsymbol{\gamma}]^\top$ where $\boldsymbol{\gamma} = [\Re(\alpha_1),\ \Im(\alpha_1),\ \tau_1,\ \delta f^a_1,\ \ldots,\ \Re(\alpha_I),\ \Im(\alpha_I),\ \tau_I,\ \delta f^a_I]^\top$ and $\boldsymbol{\theta}_p = [x,\ y,\ z,\ v_x,\ v_y,\ v_z,\ \delta f^c]^\top$. Define $\boldsymbol{T}_{\text{total}} \triangleq \frac{\partial\tilde{\boldsymbol{\eta}}_{\text{ch}}}{\partial\tilde{\boldsymbol{\eta}}^n_{\text{state}}} \in \mathbb{R}^{4I\times N_n}$, where $N_n \in \{N_u, N_b\}$ is the state vector length, with $N_u = 4I+7$ and $N_b = 4I$. The overall FIM in the state domain is then $\boldsymbol{J}^{\text{total}}_{\text{state}} = \boldsymbol{T}^\top_{\text{total}}\boldsymbol{J}^{\text{total}}_{\text{ch}}\boldsymbol{T}_{\text{total}}$.

B. Common-Mode Error Mitigation via Correlated Information

Let $\boldsymbol{J}_{\text{state}}^{\text{UT}}$ denote the UT's Fisher Information Matrix (FIM), derived from Doppler-only observations, and let $\boldsymbol{J}_{\text{state}}^{\text{BS}}$ be the corresponding FIM at the BS.

Although the UT cannot directly observe the BS measurements, information can still be transferred due to the spatial correlation between the atmospheric effects seen at the BS and those at the UT. In particular, we assume the UT's unknown atmospheric frequency bias parameter δf^a is correlated with that of the BS. We model this as a linear relationship of the form $\delta f_{\text{UT}} \approx \rho(d_{bu})\, \delta f_{\text{BS}}$, where $\rho(d_{bu}) \in [0,1]$ is a known spatial correlation function that decays with the distance d_{bu} between the UT and BS. This correlation allows us to compute an induced information contribution from the BS to the UT frequency bias estimate. This results in an effective "prior-like" contribution to the UT's FIM, given by

$$\boldsymbol{J}_{\text{induced}} = \begin{bmatrix} \mathbf{0}_{10\times 10} & 0 \\ 0 & J_f \end{bmatrix},$$

where,

$$J_f = \rho(d_{bu})^2 \cdot J_{\text{state}}^{\text{BS}}(i_f, i_f). \tag{15}$$

Here, i_f denotes the index of δf^a within the BS state vector. $\rho(d_{bu})$ is the correlation coefficient (defined in (17)), and its square reflects the proportion of transferable information based on the assumed linear relationship between UT and BS frequency biases.

The augmented FIM at the UT, incorporating this induced information, becomes

$$\boldsymbol{J}_{\text{state}}^{\text{aug}} = \boldsymbol{J}_{\text{state}}^{\text{UT}} + \boldsymbol{J}_{\text{induced}}. \tag{16}$$

This formulation does not rely on a probabilistic prior, but rather on an information-theoretic transfer of estimation precision through spatial correlation.

We model the baseline decorrelation using an exponential decay function[2] with e-folding correlation length L_c over the horizontal separation distance d_{bu} between the BS and UT [10], [11]

$$\rho(d_{bu}) = \exp\left(-\frac{d_{bu}}{L_c}\right). \tag{17}$$

[2]In practice, the correlation decay rate in $\rho(d_{bu})$ varies depending on the physical source of the impairment. Both tropospheric and ionospheric effects decorrelate with increasing horizontal baseline, but at different rates. The tropospheric delay typically exhibits a shorter correlation length, on the order of 5–10 km, while the ionospheric delay tends to decorrelate over longer distances, typically 20–50 km. To ensure robustness and avoid overestimating the benefit of shared information, we conservatively select the smaller of the two as the correlation length L_c.

IV. Simulation Setup and Results

A. Simulation Setup

a) Satellite Orbit Modeling: For realistic Doppler observations, we model each LEO satellite as moving on a circular orbit of fixed altitude a above an idealized spherical Earth of radius R_e. Specifically, for the i^{th} satellite, we draw a random unit vector $\boldsymbol{q}_i \in \mathbb{S}^2 \subset \mathbb{R}^3$, uniformly distributed on the two-dimensional unit sphere, and set its ECEF position to $\boldsymbol{r}_{\text{s}}^{(i)} = (R_e + a)\, \boldsymbol{q}_i$. To ensure satellite visibility from both the UT and the BS, we retain only those samples for which the elevation angle with respect to both receivers exceeds a certain elevation mask (e.g., 10°). Under the circular-orbit assumption, the satellite's speed is $v_{\text{orb}} = \sqrt{\frac{\mu}{R_e+a}}$, where μ is Earth's gravitational parameter. To obtain a velocity vector perpendicular to the radius, we choose an arbitrary unit-norm "orbit normal" $\mathbf{n}_i$, form the cross-product $\boldsymbol{v}_{\text{dir,i}} = \boldsymbol{n}_i \times \boldsymbol{q}_i$, normalize it, and assign $\boldsymbol{v}_{\text{s}}^{(i)} = v_{\text{orb}} \frac{\boldsymbol{n}_i \times \boldsymbol{q}_i}{\|\boldsymbol{n}_i \times \boldsymbol{q}_i\|}$. This simple geometric construction yields self-consistent ECEF position and velocity vectors for each LEO satellite, which we then use to compute the UT and BS ranges and range-rates (Doppler shifts).

b) Simulation Parameters: Table I summarizes the simulation parameters, including the LEO satellite orbit, satellite signal characteristics, receiver configuration, and atmospheric error model parameters. Three sets of Monte Carlo simulations were conducted, showing the impact of received SNR, number of satellites, and baseline distances between the BS and UT. The reported root mean squared errors (RMSE) are averaged over 1000 independent trials to ensure statistical reliability.

B. Results and Discussions

a) Performance bounds of classical and differential Doppler-only positioning: Figure 1 shows the RMSE of frequency bias, 3D velocity, and 3D position estimation as a function of SNR for both classical and differential positioning methods. As expected, the differential method consistently outperforms the classical method, particularly at lower SNR values. Both methods exhibit a decrease in RMSE as SNR increases, with the performance nearly converging at higher SNR. While these results highlight the clear benefit of differential Doppler processing, it is important to recognize their practical implications. The position error bounds observed may be acceptable for applications such as large-scale logistics tracking or maritime positioning, but are too coarse for safety-critical use cases like autonomous driving, where sub-meter accuracy is typically required. In such scenarios, additional measurements (e.g., time-of-arrival) must be integrated to achieve sufficient accuracy. Furthermore, the assumption of having simultaneous access to 10 or more LEO satellites from a single constellation may be optimistic under current satellite deployment densities, and thus represents a best-case scenario that may not yet be achievable in practice—unless a

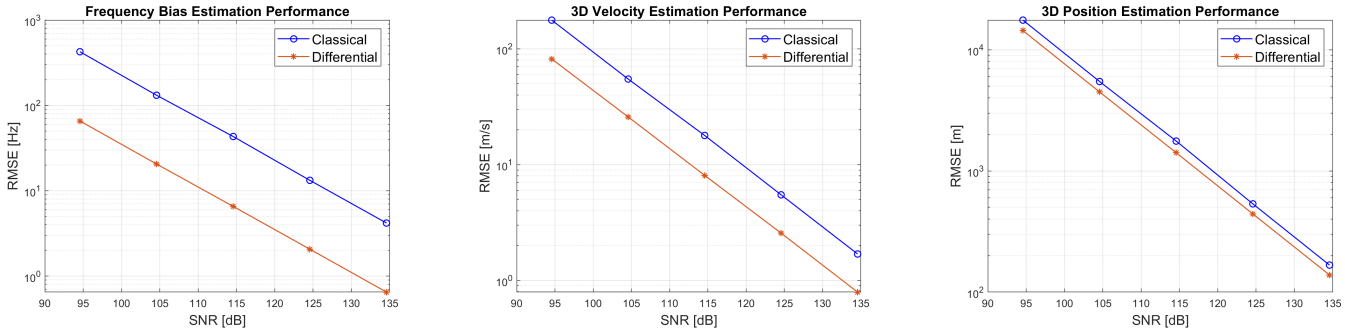

(a) (b) (c)

Fig. 1: CRLB performance of (a) frequency bias, (b) 3D velocity, and (c) 3D position estimation as a function of SNR.

TABLE I: Simulation Parameters

Block	Parameter	Value
LEO orbit	Orbital altitude a	600 km
	Earth radius R_e	6371 km
	Gravitational param. μ	3.986×10^{14} m^3/s^2
	Orbital speed v_{orb}	7561 m/s
	# of satellites I	10
	Elevation mask	10°
LEO Signal	Carrier freq. f_c	2 GHz
	Subcarrier spacing Δf	60 kHz
	# subcarriers K	720
	# OFDM symbols L	252
	Bandwidth $B = K\,\Delta f$	60 MHz
	Cyclic prefix duration T_{cp}	7% T
	Transmit power	54 dBm
	Antenna gain	10 dBi
Receiver	UT position $\boldsymbol{r}_u$	$[(R_e + 1.5),\ 0,\ 0]$ m
	BS position $\boldsymbol{r}_b$	$\boldsymbol{r}_u$ + $[8.5,\ y,\ 0]$ m
	UT velocity $\boldsymbol{v}_u$	$[0.3,\ 5.2,\ 6.7]$ m/s
	BS velocity $\boldsymbol{v}_b$	$[0,\ 0,\ 0]$ m/s
	Antenna gain (BS/UT)	0 dBi
	Noise figure NF	7 dB
Atmosphere	TEC rate $\dot{\text{TEC}}_0$	0.001 TECU/s
	Correlation length L_c	10 km
	Zenith wet-delay rate $\dot{Z}_{w,0}$	1×10^{-7} m/s
	Water-vapour scale height H	2000 m

multi-constellation solution is considered, which could improve visibility and coverage.

b) Impact of baseline distance: Figure 2 illustrates the RMSE for frequency bias, 3D velocity, and 3D position estimation as a function of the BS-UT baseline. Both classical and differential positioning methods are compared. As expected, the classical performance bound is independent of the baseline distance. The bounds of the differential Doppler approach, on the other hand, increases with baseline, as atmospheric corrections become uncorrelated between the two receivers. It is also observed that, at the 50 km mark, the two methods attain identical bounds. However, communications between the two receivers will cease way before that.

c) Estimation Performance with Varying Number of Satellites: Figure 3 shows the CRLB performance for state estimation as a function of the number of satellites. The RMSE for both classical and differential methods decreases with an increasing number of satellites. The differential method, however, consistently outperforms the classical method, particularly as the number of satellites increases. It is evident that differential frequency bias estimation remains unchanged with the number of satellites, as the frequency bias is a global error (for each satellite) that affects both receivers equally, and therefore, adding more satellites does not influence the cancellation of this error (after BS information fusion). Once the differential measurement has accounted for the common-mode errors, the performance in frequency bias estimation reaches a saturation point. Consequently, increasing the number of satellites does not lead to further improvement in frequency bias estimation accuracy. Nevertheless, increasing the number of satellites yields a significant improvement in both 3D velocity and 3D position estimation. This enhancement arises from the greater number of measurements, and better geometric dilution of precision (GDOP), thereby leading to more accurate estimation of these parameters.

V. Conclusion

In this paper, we have analyzed the theoretical limits of differential Doppler positioning using LEO satellite signals. We compared the performance of classical Doppler-only positioning with that of a differential approach that incorporates additional measurements from a stationary base station. Through simulation and analysis, we quantified the impact of various factors such as SNR, baseline distance between the base station and the user terminal, and atmospheric error models on the positioning performance. The results show that the differential Doppler positioning approach significantly outperforms the classical method, particularly in low-SNR scenarios. At high SNR and short baseline, both methods converge, but the differential approach consistently maintains an edge in accuracy. Future work will focus on examining the impact of multipath

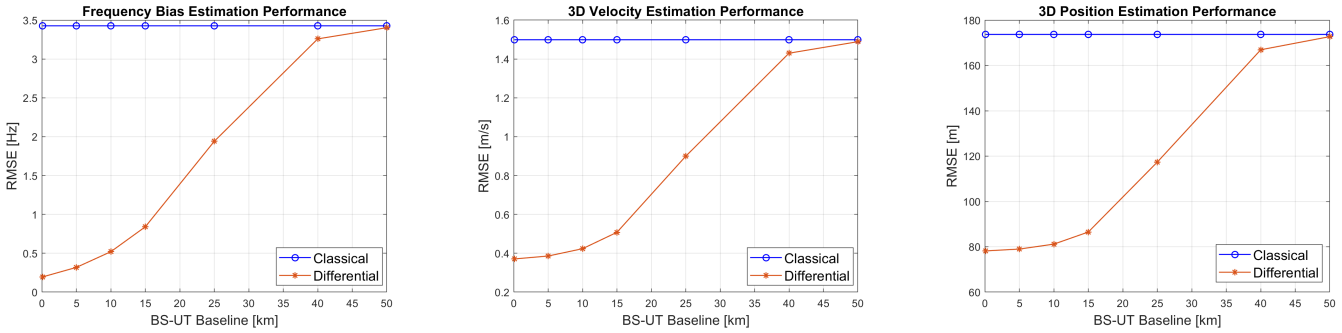

(a) (b) (c)

Fig. 2: CRLB performance of (a) frequency bias, (b) 3D velocity, and (c) 3D position estimation as a function of BS-UT baseline.

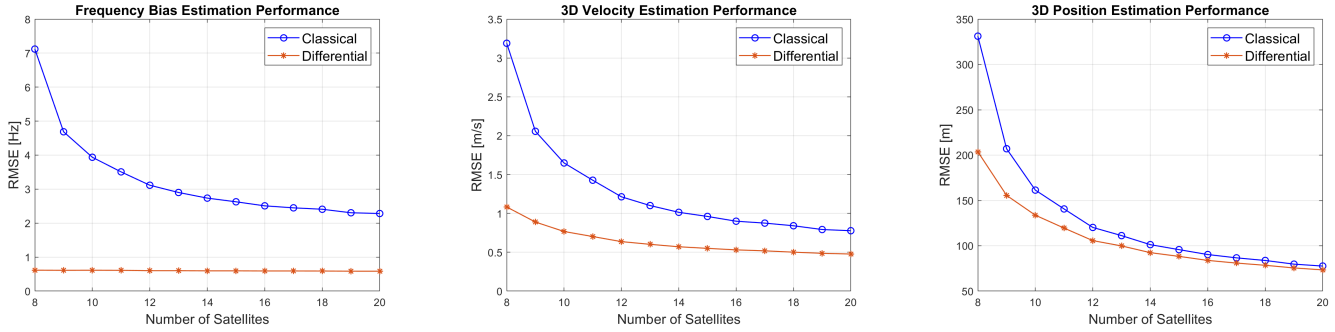

(a) (b) (c)

Fig. 3: CRLB performance of (a) frequency bias, (b) 3D velocity, and (c) 3D position estimation as a function of the number of satellites.

interference on both classical and differential Doppler-only positioning. Additionally, it will consider dynamic scenarios with advanced atmospheric modeling, investigating the temporal and spatial variability of atmospheric effects. Building on the CRLB framework developed in this work, future research will also explore the design and evaluation of practical estimators that approach these theoretical bounds.

REFERENCES

[1] H. Benzerrouk, Q. Nguyen, F. Xiaoxing, A. Amrhar, H. Rasaee, and R. J. Landry, "LEO satellites based Doppler positioning using distributed nonlinear estimation," *IFAC-PapersOnLine*, vol. 52, no. 12, pp. 496–501, 2019, 21st IFAC Symposium on Automatic Control in Aerospace ACA 2019.

[2] C. Shi, Y. Zhang, and Z. Li, "Revisiting Doppler positioning performance with LEO satellites," *GPS Solutions*, vol. 27, no. 1, p. 126, 2023.

[3] C. Zhao, H. Qin, N. Wu, and D. Wang, "Analysis of baseline impact on differential Doppler positioning and performance improvement method for LEO opportunistic navigation," *IEEE Transactions on Instrumentation and Measurement*, vol. 72, p. 8501110, 2023.

[4] M. Jiang, H. Qin, Y. Su, F. Li, and J. Mao, "A design of differential-low earth orbit opportunistically enhanced GNSS (D-LEOGNSS) navigation framework," *Remote Sensing*, vol. 15, no. 8, p. 2136, 2023.

[5] J. Saroufim, S. Hayek, and Z. M. Kassas, "Simultaneous LEO satellite tracking and differential LEO-aided IMU navigation," in *Proceedings of the IEEE/ION Position, Location and Navigation Symposium (PLANS)*, 2023, pp. 179–188.

[6] M. Ji, R. Luo, N. Xu, Y. Li, and X. Chen, "An opportunistic LEO-based Doppler differential positioning method with baseline optimization," in *Proceedings of the 2023 International Conference on Communication Network and Machine Learning*, ser. CNML '23. New York, NY, USA: Association for Computing Machinery, 2024, p. 123–128.

[7] S. Shahcheraghi, J. Saroufim, and Z. M. Kassas, "Acquisition, Doppler tracking, and differential LEO-aided IMU navigation with uncooperative satellites," *IEEE Aerospace and Electronic Systems Magazine*, pp. 1–15, 2025.

[8] H. Sallouha, S. Saleh, S. De Bast, Z. Cui, S. Pollin, and H. Wymeersch, "On the ground and in the sky: A tutorial on radio localization in ground-air-space networks," *IEEE Communications Surveys Tutorials*, vol. 27, no. 1, pp. 218–258, 2025.

[9] M. R. Imad, "Atmospheric effects on satellite navigation systems," *atmosphere*, 2024.

[10] A. Klos, J. Bogusz, R. Pacione *et al.*, "Investigating temporal and spatial patterns in the stochastic component of ztd time series over europe," *GPS Solutions*, vol. 27, no. 1, p. 19, 2023.

[11] K. Wang, A. El-Mowafy, Q. Weijin, and X. Yang, "Integrity monitoring of PPP-RTK positioning; part I: GNSS-based IM procedure," *Remote Sensing*, vol. 14, p. 44, 12 2021.

[12] J. A. Klobuchar, "Ionospheric time-delay algorithm for single-frequency GPS users," *IEEE Transactions on Aerospace and Electronic Systems*, vol. AES-23, no. 3, pp. 325–331, 1987.

[13] J. Saastamoinen, "Atmospheric correction for the troposphere and stratosphere in radio ranging of satellites," in *The Use of Artificial Satellites for Geodesy*, ser. Geophysical Monograph Series. American Geophysical Union, 1972, vol. 15, pp. 247–251.